Chemical Engineering & Processing: Process Intensification 145 (2019) 107682

Contents lists available at ScienceDirect

Chemical Engineering & Processing: Process Intensification

journal homepage: www.elsevier.com/locate/cep

Evaluation of mechanical vapor recompression crystallization process for treatment of high salinity wastewater

H. Dahmardeh, H.A. Akhlaghi Amiri*, S.M. Nowee

Chemical Engineering Department, Faculty of Engineering, Ferdowsi University of Mashhad, Mashhad, Iran

ARTICLE INFO

Keywords:
Desalination
Wastewater
Mechanical vapor recompression
Single and multi-effect evaporation
Crystallization

ABSTRACT

Single/multiple-effect evaporation (SEE/MEE) along with single/multi-stage mechanical vapor recompression (SVR-MVR) systems were simulated for high salinity wastewater treatment. They were optimized for feed salinity of 70 g/kg and zero liquid discharge (i.e., salt saturation concentration of 285 g/kg). The compressor specific power consumption (e.g., 0.193–0.064 kWh/kg for SEE-SVR) and the required heat transfer surface areas of the evaporator (e.g., 2719.78–498.01 m^2 for SEE-SVR) decreased by increasing the evaporating temperature (from 50 to 90 °C), depending on the temperature difference between the condensing vapor and the boiling brine (ΔT). An optimum value was obtained for ΔT (almost 3 °C for SEE-SVR) to target either lower power consumption and heat transfer surface area. Operational expenditures (OPEX) showed a minimum at the feed salinity of 70 g/kg. The feed containing $CaCl_2$ needed more treatment energy, compared to NaCl and $MgCl_2$. Among the simulated systems, MEE-SVR showed the best performance, in terms of energy consumption and OPEX. So, the optimized MEE-SVR system was combined with a crystallization unit for better water recovery and solid salt removal from high salinity wastewater. Increment of the feed salinity caused decreased mean crystal size by raising nucleation rate and reducing growth rate.

1. Introduction

A desalting/dehydration plant (DDP) is often installed in crude oil production units, in order to remove water-soluble salts from the produced oil [1]. DDPs are always necessary to enhance the quality of the transported crude oil; since, an increase of one ppm of brine in a barrel of crude oil considerably reduces its price [2]. They are also crucial to minimize the energy requirement for oil pumping, transportation and fouling problems in pipes and to prevent formation of hydrochloric acid, which is extremely corrosive, and metallic salts, which could deactivate catalysts during oil processing [2,3]. The two biggest challenges associated with DDPs in the world are massive wastewater production, which may be up to three times the produced oil volume [4,5], and dilution (wash) water consumption, which is approximately 1–10% of the inlet oil volume [6]. The wastewater from DDPs mostly contains NaCl, $CaCl_2$ and $MgCl_2$, oil and grease [4]. Therefore, due to the environmental concerns, such a wastewater cannot be released into the environment, so it is normally re-injected into the reservoir [7]. However, its high salinity often destroys the injection facilities such as the valves and pumps. The amount of total dissolved solids (TDS) of wastewater produced from some DDPs of Iranian crude oil, as an instance, exceeds 150,000 ppm [4], so the need for treatment of such DDP's wastewater is raised.

The choice of treatment method depends on TDS content of the treated wastewater [6]. Among conventional wastewater treatment techniques (e.g., reverse osmosis (RO) [8,9], nanofiltration (NF) [10,11], electrodialysis [12,13], multi effect evaporation (MEE) [14,15] and multi-stage flashing (MSF) [15,16]), evaporation methods are known as more effective ones, due to their simplicity of pretreatment, higher product purity and longer life of the separating surface [17,18]. However, current evaporation techniques require a large amount of the external heating sources and their operation is also complex [7,19]. Mechanical vapor recompression (MVR) is one of the evaporation techniques which is able to treat highly concentrated wastewater [19] with less vapor consumption, compared to the other methods. In MVR, the produced vapor from the evaporator is compressed and reused in the process [19]. Moreover, its other advantages could be addressed namely as simple and reliable operation; low-temperature operation; high product purity; compact equipment, which does not require an external heating source; high thermodynamic efficiency and low corrosion rate [20–22].

MVR systems have been developed since 1970s, mostly for seawater desalination [20,23]. Reported studies in literature involve design, thermal performance and energy analysis [24,25], experimentation

* Corresponding author.
E-mail address: ha.akhlaghi@um.ac.ir (H.A. Akhlaghi Amiri).

https://doi.org/10.1016/j.cep.2019.107682
Received 18 July 2019; Received in revised form 3 October 2019; Accepted 6 October 2019
Available online 11 October 2019
0255-2701/

Nomenclature

A	heat transfer area, m^2
CAPEX	capital expenses, kUS$ $year^{-1}$
Cc	cost parameter for the cooling services, (US$ (kW year) $^{-1}$
Cp	specific heat, kJ $(kg\,K)^{-1}$
Ec	cost parameter for electricity, US$ (kW year)$^{-1}$
F	mass flowrate, $kg\,s^{-1}$
H	specific enthalpy, $kJ\,kg^{-1}$
LMTD	logarithmic mean temperature difference
OPEX	operational expenses, kUS$ $year^{-1}$
Q	heat transfer rate, kW
T	temperature, °C
U	overall heat transfer coefficient, $kWm^{-2}\,K^{-1}$
W	compression power, kW

Subscripts

b	brine
c	condensate
e	evaporator
i	evaporator effects
j	compressor stages
v	superheated vapor
cv	condensate vapor

Superscript

s	sensible

Acronyms

MEE	multiple-effect evaporation
MSF	multistage flash
MVR	mechanical vapor recompression
MVRC	mechanical vapor recompression crystallization
RO	reverse osmosis
SEE	single-effect evaporation
SVR	single-stage vapor recompression
TDS	total dissolved solids
ZLD	zero liquid discharge

[26,27] and economic evaluation [28,29] of MVR systems. At the beginning, single – effect MVR was popular; however, later, different applications of MVR in c[Lukic, 2010 #103]ombination with other systems, such as multi-stage flash (MSF) [30], MEE [30,31] and reverse osmosis (RO) [32], were developed. A single-effect MVR system has a high energy consumption to treat high salinity wastewaters [19]. Using a constant pressure evaporator, increasing the salt concentration, results in higher compressor power consumption; as the boiling point of the solution increases [33]. Therefore, in order to reduce the compressor power, first a part of the inlet wastewater stream is pre-evaporated at lower concentration. Then, the final evaporation takes place at a condition very close to salt saturation point (300,000 ppm or 300 g kg^{-1}). This is the basis of the double-effect mechanical vapor compression [19,34], which are now widely used in water treatments. Recently, MVR has been widely applied in treatment of shale-gas flowback water [35–39]. Other reported applications include separating N, N-Dimethylacetamide/water [40], Dimethylformamide/water [41], and acetone / methanol mixtures [42]. MVR systems may also be driven by renewable energy sources, such as wind [43] or solar [44].

Since MVR systems normally operate at saturated conditions, the outlet streams of these systems are highly concentrated [19]. To overcome this drawback, zero-liquid discharge (ZLD) condition was proposed for MVR effluent; in which all the wastewater is purified and recycled. MVR with crystallization (MVRC) system, is one of those methods [45,46] which recycles the total liquid waste by producing a dry cake material from its crystallizer, which is disposed or used in other applications. In the crystallization unit, the slurry is sent to a crystallizer and is also centrifuged to separate solid particles from the liquid phase [19]. Therefore, MVRC systems reduce either the amount of needed make-up water, by approximately 100% recycling, and potential environmental risks, such as contamination of groundwater aquifers [46]. However, one can hardly find studies on this system in literature.

In the present study, different types of MVR systems, resulted by combination of single- and multi-effect evaporation with single- and multi-stage recompression, were simulated and optimized, using Aspen Plus simulation software, for application in treatment of high salinity wastewater of crude oil desalting units. These systems were evaluated and the most efficient one was selected, using different sensitivity studies on the effective parameters. Then, the selected system was combined with a crystallization unit to study the performance of the formed MVRC system under different operational conditions. The energy consumption and the operating costs of the systems were compared.

2. Simulation method

ASPEN PLUS software was selected to simulate different processes in this study and to analyze the energy consumptions. ASPEN PLUS is able to simulate steady-state processes in various industries and contains many databases including physical, chemical and thermodynamic properties of electrolyte solutions and interaction parameters for many electrolyte systems [47].

In this work, the main assumptions considered for simulation of different MVR systems are as follow:

- The processes are steady state,
- The required energy to start the processes is negligible,
- Heat losses and pressure drops in all the simulated equipments are negligible,
- There is no non-condensable gas,
- The concentrated wastewater leaving from the last evaporator effect is saturated in liquid phase,
- Total annual costs of the pumps and the mixers are negligible,

The thermodynamic package of ELCNTRL-electrolytes was deployed in the simulations, which is recommended for modeling electrolyte systems [47]. An initial mean value of 70,000 ppm (or 70 g kg^{-1}) was considered for feed salinity in the simulated MVR systems [14], being about half of the reported value in some DDPs in Iran. Most importantly, concentrated discharge salinity was to be equal to 285 g kg^{-1}; in order to achieve the operating conditions of the inlet to the ZLD system. Table 1 presents other assumptions and input data used in the simulations.

The accuracy of the simulated MVR systems was verified by comparing the results with those from the proposed mathematical model by Onishi et al. [34], for the optimal design of SEE/MEE systems. A good agreement was observed (less than 1% error) between different results, including inlet and outlet pressures and temperatures, mass flow rates, work capacities or heat transfer rates of all equipment of the simulation and the model. It was also compared with the mathematical model of Zhou et al. [48] and showed good agreement, which will be discussed in the next section.

Table 1
Input data for the simulated case studies.

Feed stream	
Flow rate	37.5 $m^3 h^{-1}$ (10.42 kg s^{-1})
Salinity	70 g kg^{-1} (NaCl)
Temperature	25 °C
Pressure	50 kPa
Multistage compressor with intercooling	
Type	Centrifugal
Isentropic efficiency	0.75
Maximum pressure ratio	3 per stage
Cost data [34]	
Electricity	850.51 US$ (kW year)$^{-1}$
Cooling services	100 US$ (kW year)$^{-1}$
Steam (120 °C @ 50 kPa)	418.8US$ (kW year)$^{-1}$

3. Results and discussion

As illustrated in Fig. 1, the simplest MVR system - i.e., single-effect evaporation process with a single-stage mechanical vapor recompression (SEE-SVR)- is composed of a compressor, a flash evaporator, a heat exchanger, brine and product pumps, and a vacuum system [19,25]. Vacuum system extracts the non-condensable gases and maintains the system pressure; so that a proper heat transfer process can be attained during the operation [25,26]. The outlet from the disposal water tank enters a preheating system maintained at the ambient temperature. The preheater is a plate-type heat exchanger, which uses the energy of products to preheat the feed wastewater. After mixing with the recycled concentrated stream, the preheated feed is pumped to tube side of a heat exchanger and turns into a hot stream. It is then partially evaporated in a flash evaporator. The generated vapor is consequently compressed to superheated steam and introduced into the shell of the heat exchanger. The sensible and the latent heat of the vapor is transferred to the mixed stream, which is flowing through the tube-side of the heat exchanger; hence, it is condensed.

In the simulated SEE-SVR process (Fig. 1), the feed wastewater was preheated (for about 600.14 kW from condensate stream) and then sent to the evaporator at 40 °C. In the evaporator, which was operated at 82.9 °C and 40 kPa, about 7.86 kg s^{-1} of the preheated stream was evaporated. Then, the generated vapor was compressed up to 72 kPa. The optimized SEE-SVR process required a compressor with of 1084.7 kW of capacity. The compressed vapor was then condensed and almost 19,887.3 kW heat was released as its temperature was reduced from 155.7 to 62.9 °C which was used to preheat the stream in the evaporator effect. Heat transfer surface area of the evaporator effects, responsible of heat transfer with and without phase change, is calculated as [34]:

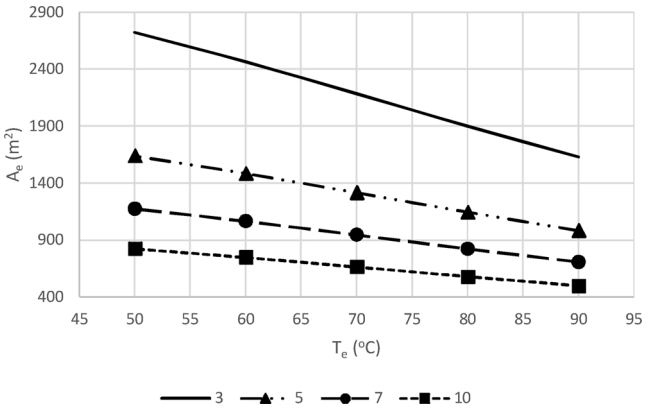

Fig. 2. Heat transfer area of the evaporator (A_e) as a function of the evaporating temperature (T_e) for different values of temperature differences between the condensing vapor and the boiling brine (ΔT).

$$A_{ei} = F_{vi}.\ Cp_s.\ \frac{T_{vj} - T_{ci}}{U^S.\ LMTD_i} + F_{vi}.\ \frac{H_{cvi} - H_{ci}}{U_i.\ (T_{ci} - T_{bi})} \quad (1)$$

where, F_{vi} is the superheated vapor mass flow rate (kg s^{-1}), Cp_s is the vapor specific heat (kJ (kg K)$^{-1}$), T_{vj} is the superheated vapor temperature (°C), T_{ci} is the condensate temperature (°C), U^S is the sensible heat transfer coefficient (kW m^{-2} K^{-1}), $LMTD_i$ logarithmic mean temperature difference, H_{cvi} is the condensate vapor specific enthalpy (kJ kg^{-1}), H_{ci} is the condensate specific enthalpy (kJ kg^{-1}), U_i is the evaporator effect overall heat transfer coefficient (kW m^{-2} K^{-1}), T_{bi} is the brine temperature (°C). The correlation for the overall heat transfer coefficient in the evaporator (U_i) is as follows [34]:

$$U_i = 0.001 \bullet (1939.4 + 1.40562 \bullet T_{bi} - 0.00207525 \bullet (T_{bi})^2 + 0.0023186 \bullet (T_{bi})^3) \quad (2)$$

Fig. 2 illustrates the dependency of the evaporator surface area (A_e) on the evaporating temperature (T_e) at different temperature differences between the condensing vapor and the boiling brine (ΔT) for the simulated SEE-SVR system. In general, at different ΔT values, A_e decreased as T_e rose up. For instance, at ΔT = 3 °C, by increasing the evaporating temperature from 50 to 90 °C, A_e almost halved. Clearly, temperature changes the physical properties of the brine and the condensing vapor, especially liquid phase viscosity; hence, the heat transfer rate of the streams was enhanced. The trends of A_e versus T_e was almost linear for all the studied cases and the slope of this decreasing trends was slightly reduced by ΔT. Obviously, at a certain T_e, lower ΔT resulted in a larger A_e and at higher ΔT values, A_e variation was decreased. Fig. 3, shows the energy consumed by the compressor per unit mass of water (W) versus T_e at different ΔT values. For all ΔT values,

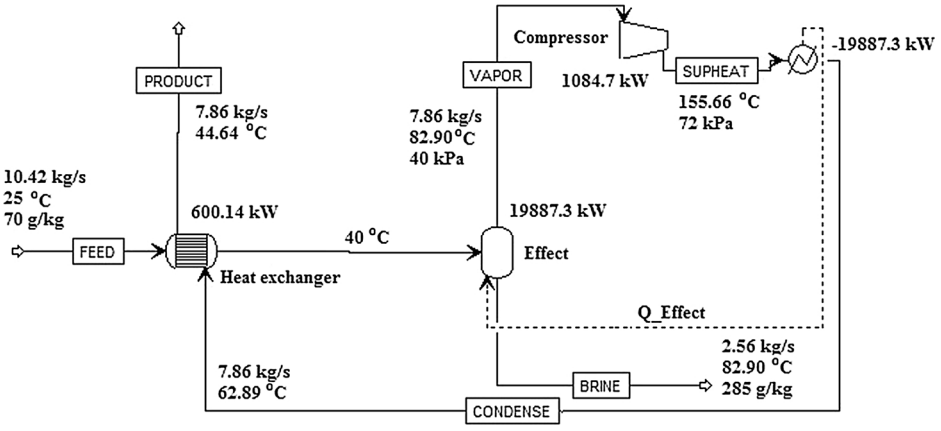

Fig. 1. Flow diagram of the simulated SEE-SVR process.

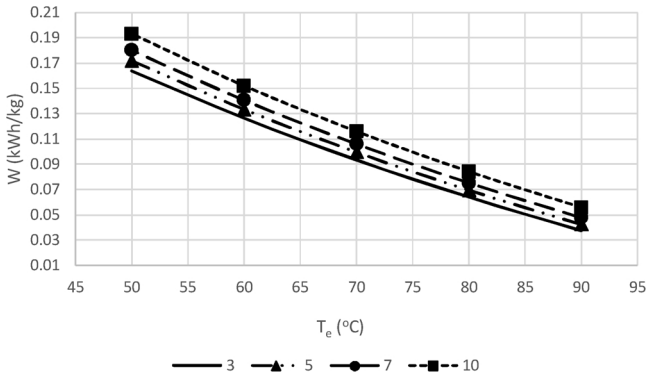

Fig. 3. Energy consumed by the compressor per unit mass of water (W) as a function of the evaporating temperature (T_e) for different values of temperature differences between the condensing vapor and the boiling brine (ΔT).

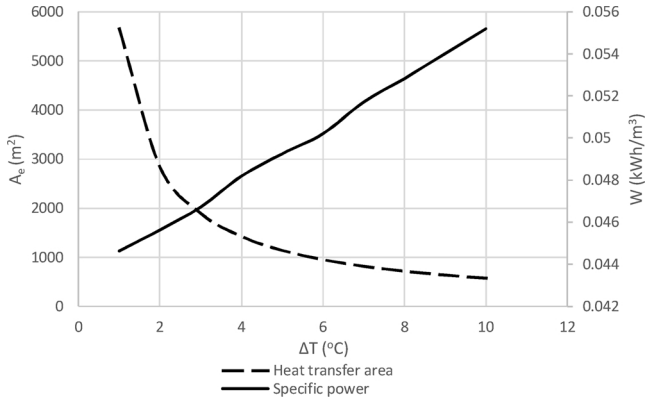

Fig. 4. Heat transfer area of the evaporator (A_e) and energy consumed by the compressor per unit mass of water (W) for different values of temperature differences between the condensing vapor and the boiling brine (ΔT) at evaporating temperature of 82.90 °C.

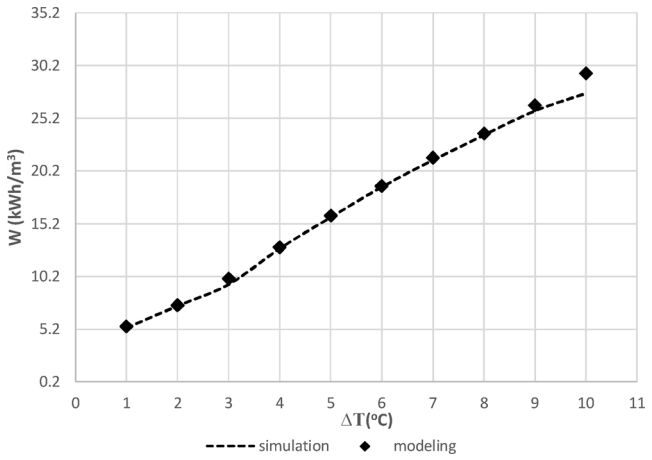

Fig. 5. Energy consumed by the compressor per unit mass of water (W) for different values of temperature differences between the condensing vapor and the boiling brine (ΔT) at evaporating temperature of 80 °C. The simulation results (dashed line) are compared with the modeling results (dots) by Zhou et al. [48].

increasing T_e resulted in less W. The observed decline in specific power consumption at higher boiling temperatures was due to decrement of compression ratio and the inlet vapor specific volume. In the simulated range of T_e (50 to 90 °C), the specific power consumption variation was less than 0.15 kW h/kg at different ΔT values. As shown in Fig. 3, at a certain T_e, W slightly increased by ΔT. Higher temperature difference between condensing and formed vapors resulted in larger compression ratio and hence higher W. By increasing evaporating temperature, the scaling problem in NaCl solution would be a concern. In order to prevent NaCl precipitation in the brine flow and also from economic point of view, the maximum evaporator temperature was set around 83 °C in the MVR system.

Fig. 4 presents the variation of A_e and W as a function of ΔT for evaporating temperature of 82.9 °C. As ΔT increased up to ΔT = 4 °C, A_e decreased rapidly to about 1000 m^2. However, for ΔT greater than 4 °C, the gradient of A_e variation reduced. W, on the other hand, increased almost linearly with ΔT. As ΔT increased from 1 to 10 °C, the specific power increased from 0.045 to 0.055 kW h/m^3. From economics point of view, a large heat transfer surface area of the evaporator would require high capital expenditures (CAPEX). Furthermore, larger specific power of the compressor would add to the operational expenditures (OPEX). Hence, based on Fig. 4, ΔT = 3 °C seems to be the optimum value for the simulated process.

To verify the accuracy of the simulated SEE-SVR system (shown in Fig. 1), a comparison was performed with the mathematical model of Zhou et al. [48]. The results of the comparison in terms of W versus ΔT are presented in Fig. 5. In this system, the feed capacity was 20 kg/h of a wastewater containing 2 wt. % Na_2SO_4. A good agreement was observed between the values obtained in this simulation and those by the model of Zhou et al. [48]; whereas a divergence occurred at ΔT > 9 °C. This difference may be attributed to the correlations used in the mathematical model formulation.

A single-effect evaporation process with a multi-stage compressor (SEE-MVR) was simulated (Fig. 6). The difference to the SEE-SVR system (Fig. 1) was a 2-stage compressor as well as its cooling service between its stages. In the simulated process, the stages of the compressor needed capacities of 320.07 kW and 725.73 kW, respectively. The compressor also needed 360.963 kW of energy for its cooler. The generated vapor with the flow rate of 7.86 kg/s was compressed by the compressor up to 72 kPa, then condensed and almost 19,887 kW heat was released as its temperature reduced from 129.17 to 50.73 °C. This energy was used to preheat the stream in the evaporator effect, with the heat transfer rate of 19,887.30 kW.

Another feasible method for lowering the compression power is to first partially pre-evaporate the water at lower concentration and then evaporate the solute at the saturation concentration. In most cases, the concentrated effluent of the first stage MVR process, goes through the second stage for more water recycling [19]. The multiple-effect evaporation with single-stage vapor recompression (MEE-SVR) was simulated (Fig. 7), in which two flashing tanks was used to separate the distillate vapor, providing a more energy recovery. In this case, the condensate stream entered the preheater at 92.21 °C in order to reuse its energy (about 1962.45 kW) for preheating the feed. The preheated stream (at 74 °C) was sent to the second evaporator. The produced vapor from the second effect evaporator was mixed with vapor stream of the second flashing tank, and then the generated vapor with the flow rate of 3.85 kg/s (at 88 °C and 60 kPa) was compressed to 144 kPa. Furthermore, the compressed vapor was condensed and about 9340.85 kW heat was released during the cooling process. This heat was deployed to preheat the stream in the first evaporator effect. On the other hand, the vapor from the first effect was mixed with the vapor stream of the first flashing tank, then it was condensed and about 9443.56 kW heat was released. The discharged excess heat was used in the second evaporator effect. In this case, the process required a compressor with capacity of 832.27 kW, without need for cooling services. The results of the current study showed good agreement with the work by Onishi et al. [34].

Fig. 8 shows the simulated multiple-effect evaporation process with multi-stage vapor recompression (MEE-MVR) system along with two flashing tanks. It is relatively similar to the simulated MEE-SVR system of Fig. 7, whereas a multi-stage compressor was used to reduce the electric power of the system. In this case, the heat transfer rate of the

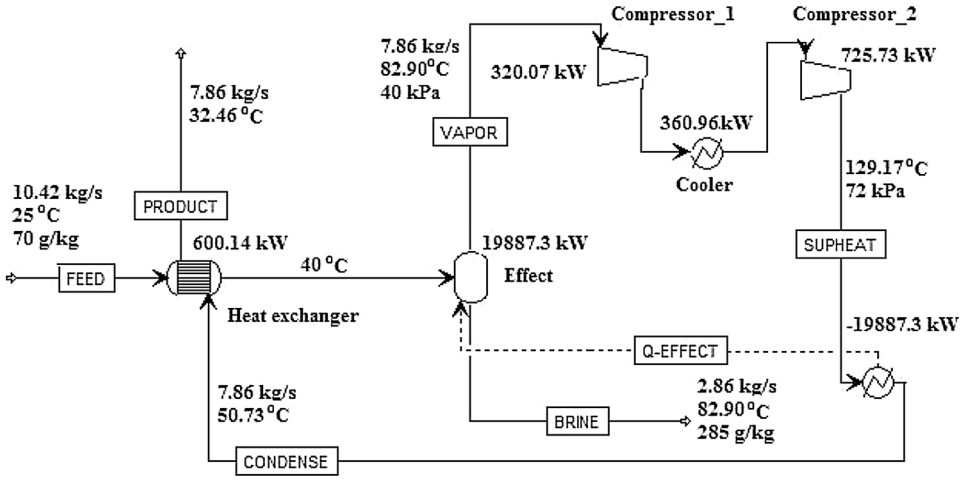

Fig. 6. Flow diagram of the simulated SEE-MVR process.

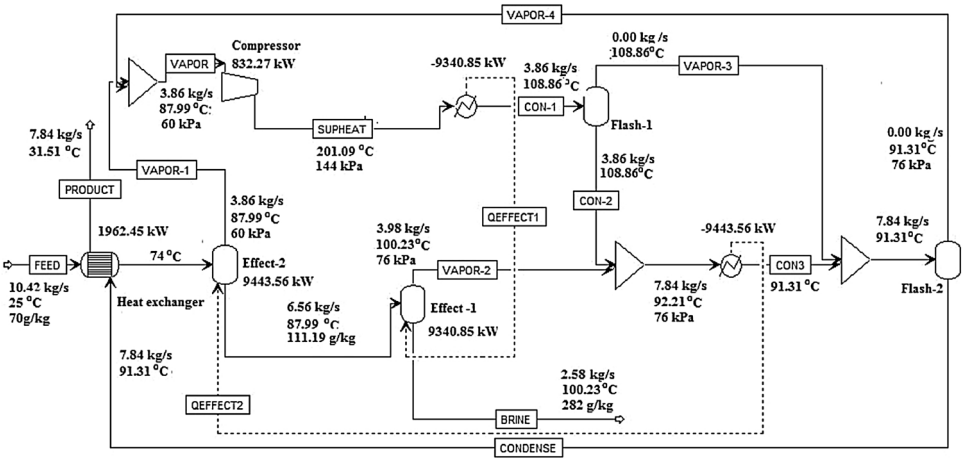

Fig. 7. Flow diagram of the simulated MEE-SVR process.

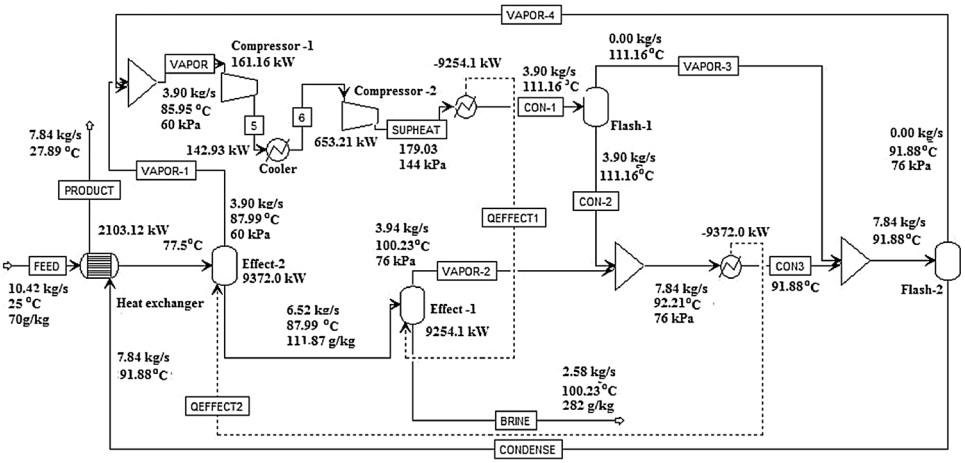

Fig. 8. Flow diagram of the simulated MEE-MVR process.

two evaporator effects were 9254.1 and 9372 kW, respectively. The process required a 2-stage compressor with capacities of 161.160 kW and 653.21 kW, respectively. This compressor demanded 142.927 kW for cooling.

The electric power consumed and the operational expenditures (OPEX) are compared for different simulated MVR systems in Fig. 9. OPEX contained the expenditures for electricity and cooling services for the multistage compressor and was calculated as follows [34]:

$$OPEX = Ec \cdot \sum_{j=1}^{2} Wj + Cc \cdot Q^{cooler} \quad (3)$$

where Ec is the cost parameter for electricity (US$ (kW year) $^{-1}$), Wj is the compression power (kW), Cc is the cost parameter for the cooling services (US$ (kW year) $^{-1}$), and Q^{cooler} is the heat transfer rate (kW). In

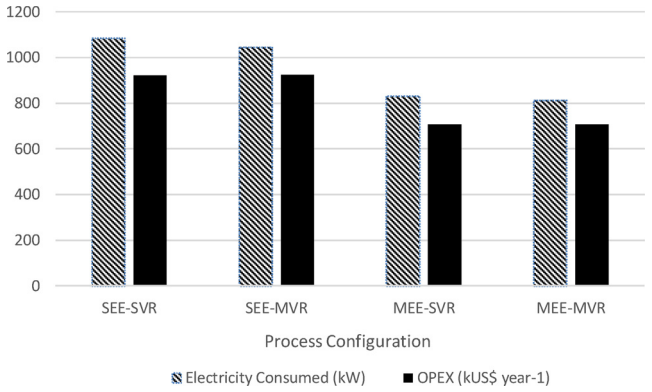

Fig. 9. Comparison between OPEX and the electrical energy consumed for different simulated processes of SEE-SVR, SEE-MVR, MEE-MVR and MEE-SVR under feed salinity of 70 g/kg.

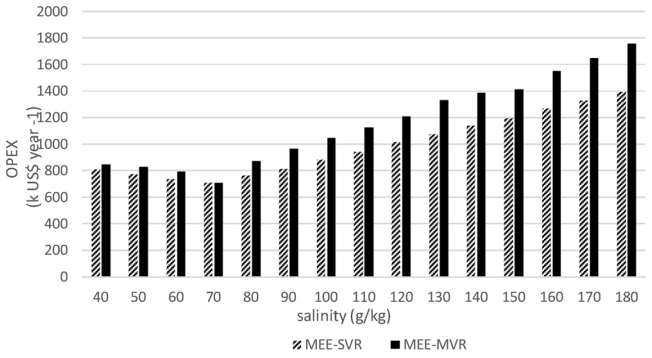

Fig. 10. Effect of the feed salinity on OPEX of MEE-SVR and MEE-MVR systems.

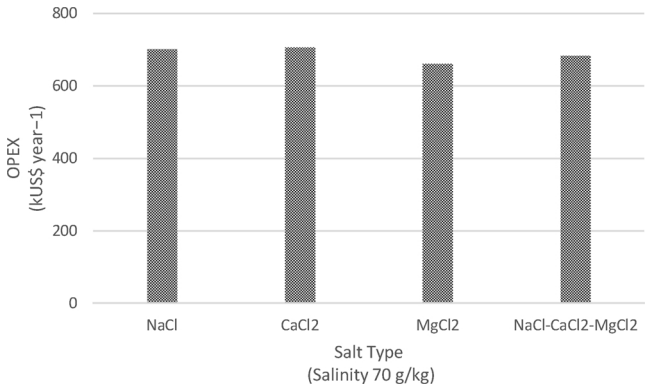

Fig. 11. Effect of salt type in the feed solution on the OPEX of the MEE-SVR system.

general, it was observed that SEE systems consumed more electrical energy and had higher OPEX than the MEE systems. Among all the simulated SEE/MEE systems, SEE-SVR showed the highest electrical energy consumption (1084 kW), while MEE-MVR system had the best performance (815 kW), from economic point of view. MEE-MVR system used 30.86% and 31.43% lower energy than the simulated SEE-MVR and SEE-SVR systems, respectively. The OPEX of SEE systems was about 925 kUS$/year, while reduced to about 707 kUS$/year for the MEE systems.

However, it should be emphasized that the evaluation results strongly depend on the feed salinity. A sensitivity study was done to assess the effect of the feed salinity on OPEX of MEE-SVR and MEE-MVR systems, as shown in Fig. 10. In general, MEE-MVR demonstrated higher OPEX than MEE-SVR in almost all the feed salt concentrations. It was also noticed that OPEX versus feed salinity had an extremum for both studied cases at salt concentration of 70 g/kg. As the feed salt concentration increased from 40 to 70 g/kg, OPEX slightly reduced to about 707 kUS$/year, which was almost the same for both systems. At lower concentrations of salt in the feed stream, larger flow rate of vapor entered the compressor; hence, the boundary condition imposed on the discharge brine salinity (i.e., 285 gkg^{-1} to remain close to ZLD conditions) resulted in a higher power consumption at lower feed salinity. As feed salinity raised above 70 g/kg, OPEX sharply escalated and became higher than 1390 and 1750 kUS$/year, for MEE-SVR and MEE-MVR systems, respectively; as the feed salinity increased to 180 g/kg. Higher salt concentration in the feed solution caused the boiling-point to rise, leading to a higher compressor power consumption and hence OPEX. At higher salinities, MEE-SVR showed considerably lower OPEX, than MEE-MVR.

Additionally, the feed brine composition may also affect the operating costs of the MVR systems. Fig. 11 presents the effect of the salt type in the feed solution on the OPEX of the simulated MEE-SVR system. In this study, the salinity of all the cases were kept equal to 70 g/kg; while, the type of the solution salts varied (i.e., NaCl, $MgCl_2$, $CaCl_2$ and a mixture of 70% NaCl, 20% $CaCl_2$ and 10% $MgCl_2$). In all cases, the discharge brine salinity remained identical in order to get close to ZLD conditions. As shown in Fig. 11, the related OPEX to electricity consumption for NaCl, $CaCl_2$, $MgCl_2$ and the mixture were 825, 830, 777 and 803 kUS$/$year^{-1}$, respectively. MEE-SVR system with $CaCl_2$ solution as the feed showed higher OPEX; which was almost 0.7%, 6.42% and 3.30% higher than the solutions contained NaCl, $MgCl_2$ and all three salts, respectively. This observation may be attributed to interactive forces between the ions in $CaCl_2$ solution which is greater than $MgCl_2$ and NaCl solutions.

3.1. Mechanical vapor recompression crystallization (MVRC) system

In the previous section, the simulation of different types of MVR systems showed that MEE-SVR for stream with salinity > 70 g/kg is the most cost-effective system, in terms of OPEX. Therefore, a case of combined MEE-SVR system with crystallization (MVRC) was designed in order to investigate the possibility of recovering more water. Fig. 12 shows the simulated MVRC system. In this case, like the MEE-SVR system, the feed solution entered the preheater, then it streamed through the second and first evaporators successively. The produced vapor from the effect evaporators was mixed, and then the generated vapor was compressed. Furthermore, the compressed vapor was condensed. This condensation heat was deployed to preheat the stream in the first evaporator effect. Moreover, the vapor from the first effect was mixed with the vapor stream of the first flashing tank, and then was condensed and heat was released as it was cooled. The discharged excess heat was used in the second evaporator effect. Eventually, the outlet brine from SEE-SVR system was sent to a crystallizer. Crystallizer models a mixed suspension, mixed product removal (MSMPR) crystallizer. Similar to the previous cases, the process required a compressor with capacity of 832.27 kW, without need for cooling service. The crystallization system needed about 3977 kW of energy for producing approximately 1.75 kg/s of steam and 0.830 kg/s of crystal (assuming 5% moisture content of the solid output), and the OPEX for this combined system was about 1665 kUS $/year, in which the steam temperature was 120 °C at 50 kPa.

Municipal applications, such as road deicing during winter, could be a purpose of crystallizing of the metal salts from DDPs. Crystal's size is particularly important when the solid product is deployed for deicing roads. Finer crystals would deice quicker, with lower efficiency; while coarser crystals take more time to take effect, with higher efficiency. Crystal size between 0–10 mm was proposed here, according to ASTM D-632 standard. Fig. 13 shows the particle size distribution of NaCl which achieved D50 of approximately 3.5 mm in the outlet stream. It was assumed that only 1% of total NaCl(s) of inlet stream to the crystallizer is present, and also about 5% moisture was considered for the

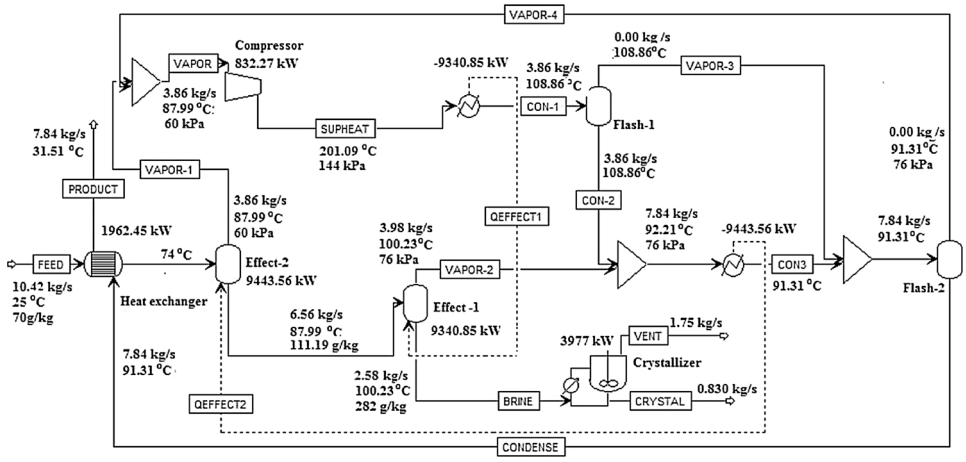

Fig. 12. Flow diagram of the simulated MVRC process.

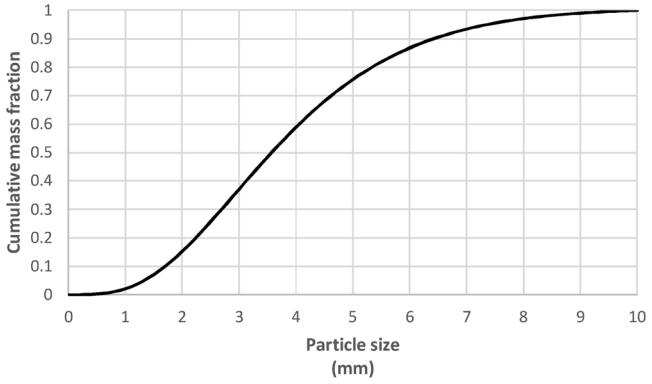

Fig. 13. Particle size distribution in the outlet stream.

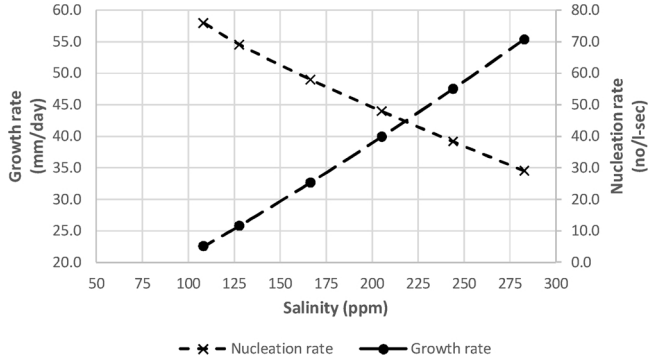

Fig. 15. Effect of the wastewater salinity on the growth rate and nucleation rate.

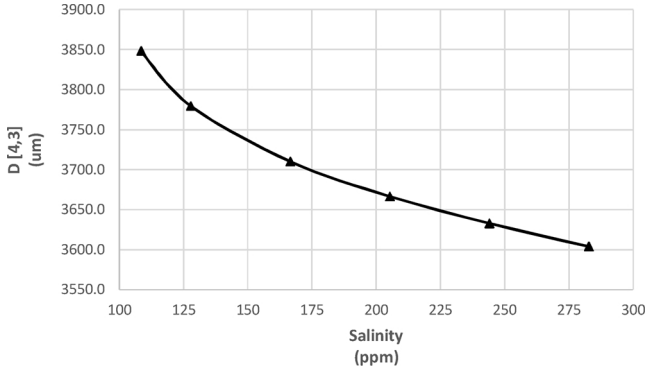

Fig. 14. Effect of the wastewater salinity on the distribution of crystals sizes.

produced crystals of outlet stream.

Fig. 14 shows the effect of the feed wastewater salinity on the mean crystal size distribution (D [4,3]) of NaCl. Increment in the inlet stream salinity decreased D [4,3] which was in accordance with the trend of growth and nucleation kinetics obtained by changing the salinity (Fig. 15). As it is clear higher salinity led to higher nucleation rates with lower growth which produced finer particles.

4. Conclusion

In this investigation, MVRC system was proposed and used to treat wastewater of DDPs. To the best of our knowledge, this is the first work proposing the MVRC process for the treatment of wastewater with a high salt content. For this purpose, the processes were built in ASPEN PLUS software and was validated with mathematical models in literature.

First, the SEE/MEE -SVR/MVR systems have been simulated and compared in terms of their applicability to achieve ZLD conditions and operating expenses. The optimal systems should achieve high recovery ratio of produced freshwater and brine remain close to ZLD condition through the specification of the outflow brine salinity (285 g/kg) by minimizing the operating expenses related to cooling services and electricity consumption.

The results showed that among all the simulated systems, the MEE-SVR system has the best performance for desalination of the wastewater, in terms of energy consumption and operational expenditures (OPEX) with feed salinity of 70 g/kg. The system required electric power and OPEX of 832.27 k US$ year−1 and 707.85 k US$ year−1 for feed salinity of 70 g/kg, respectively.

A sensitivity analysis was performed to assess the impact of feed salinity and composition on the system performance and the process costs. The simulation results revealed that the proposed system strongly depend on the treated wastewater salinity. Moreover, the analysis showed that the MEE-SVR was the most beneficial system for treatment of feed with salinity above 70 g/kg, so it was chosen as the final system for simulating with crystallization system (MVRC). In addition, the feed containing $CaCl_2$ needed more treatment energy compared to water containing NaCl, $MgCl_2$ and mixture of all three salts (70% NaCl, 20% $CaCl_2$ and 10% $MgCl_2$), while the feed salinity of all cases was 70 g/kg.

Finally, the simulation results of the MVRC showed that the particle size distribution of sodium chloride achieved D 50 of approximately 3.55 mm and also the moisture for the crystals produced in the outlet stream was about 5%. In addition, increasing feed wastewater salinity caused decrement of mean crystal size (D [4,3]) and increased crystal growth rate (decreased nucleation rate).

Declaration of Competing Interest

The authors declare that they have no known competing financial interests or personal relationships that could have appeared to influence the work reported in this paper.

References

[1] S. Abdul-Wahab, et al., Building inferential estimators for modeling product quality in a crude oil desalting and dehydration process, Chem. Eng. Process. Process. Intensif. 45 (7) (2006) 568–577.
[2] F.S. Manning, et al., Oilfield Processing, Vol. 2: Crude Oil Vol. 2 Pennwell, Tulsa, Oklahoma, 1995.
[3] L. Vafajoo, K. Ganjian, M. Fattahi, Influence of key parameters on crude oil desalting: an experimental and theoretical study, J. Pet. Sci. Eng. 90–91 (2012) 107–111.
[4] A. Pak, T. Mohammadi, Wastewater treatment of desalting units, Desalination 222 (1) (2008) 249–254.
[5] A. Fakhru'l-Razi, et al., Review of technologies for oil and gas produced water treatment, J. Hazard. Mater. 170 (2) (2009) 530–551.
[6] M. Al-Otaibi, et al., Experimental investigation of crude oil desalting and dehydration, Chem. Eng. Commun. 190 (1) (2003) 65–82.
[7] J. Daniel Arthur, et al., Technical Summary of Oil & Gas Produced Water Treatment Technologies, (2005).
[8] A. Malek, M.N.A. Hawlader, J.C. Ho, Design and economics of RO seawater desalination, Desalination 105 (3) (1996) 245–261.
[9] S.A. Avlonitis, K. Kouroumbas, N. Vlachakis, Energy consumption and membrane replacement cost for seawater RO desalination plants, Desalination 157 (1) (2003) 151–158.
[10] C. Kaya, et al., Pre-treatment with nanofiltration (NF) in seawater desalination—-preliminary integrated membrane tests in Urla, Turkey, Desalination 369 (2015) 10–17.
[11] D. Zhou, et al., Development of lower cost seawater desalination processes using nanofiltration technologies—a review, Desalination 376 (2015) 109–116.
[12] H.-J. Lee, et al., Designing of an electrodialysis desalination plant, Desalination 142 (3) (2002) 267–286.
[13] K. Tado, et al., An analysis on ion transport process in electrodialysis desalination, Desalination 378 (2016) 60–66.
[14] F.N. Alasfour, M.A. Darwish, A.O. Bin Amer, Thermal analysis of ME—TVC + MEE desalination systems, Desalination 174 (1) (2005) 39–61.
[15] G. Raluy, L. Serra, J. Uche, Life cycle assessment of MSF, MED and RO desalination technologies, Energy 31 (13) (2006) 2361–2372.
[16] R. Borsani, S. Rebagliati, Fundamentals and costing of MSF desalination plants and comparison with other technologies, Desalination 182 (1) (2005) 29–37.
[17] A. Subramani, J.G. Jacangelo, Emerging desalination technologies for water treatment: a critical review, Water Res. 75 (2015) 164–187.
[18] S. Burn, et al., Desalination techniques—a review of the opportunities for desalination in agriculture, Desalination 364 (2015) 2–16.
[19] L. Liang, et al., Treatment of high-concentration wastewater using double-effect mechanical vapor recompression, Desalination 314 (2013) 139–146.
[20] H. Ettouney, H. El-Dessouky, Y. Al-Roumi, Analysis of mechanical vapor compression desalination process, Int. J. Energy Res. 23 (1999) 431–451.
[21] M.A. Darwish, Thermal analysis of vapor compression desalination system, Desalination 69 (3) (1988) 275–295.
[22] F. Al-Juwayhel, H. El-Dessouky, H. Ettouney, Analysis of single-effect evaporator desalination systems combined with vapor compression heat pumps, Desalination 114 (3) (1997) 253–275.
[23] M. Lucas, B. Tabourier, The mechanical vapour compression process applied to seawater desalination: a 1,500 ton/day unit installed in the nuclear power plant of Flamanville, France, Desalination 52 (2) (1985) 123–133.
[24] F.N. Alasfour, H.K. Abdulrahim, The effect of stage temperature drop on MVC thermal performance, Desalination 265 (1) (2011) 213–221.
[25] H. Ettouney, Design of single-effect mechanical vapor compression, Desalination 190 (1) (2006) 1–15.
[26] N.H. Aly, A.K. El-Figi, Mechanical vapor compression desalination systems—a case study, Desalination 158 (1) (2003) 143–150.
[27] R. Bahar, M.N.A. Hawlader, L.S. Woei, Performance evaluation of a mechanical vapor compression desalination system, Desalination 166 (2004) 123–127.
[28] N. Lukic, et al., Economical aspects of the improvement of a mechanical vapour compression desalination plant by dropwise condensation, Desalination 264 (1) (2010) 173–178.
[29] A.S. Nafey, H.E.S. Fath, A.A. Mabrouk, Thermoeconomic design of a multi-effect evaporation mechanical vapor compression (MEE–MVC) desalination process, Desalination 230 (1) (2008) 1–15.
[30] A.A. Mabrouk, A.S. Nafey, H.E.S. Fath, Analysis of a new design of a multi-stage flash–mechanical vapor compression desalination process, Desalination 204 (1) (2007) 482–500.
[31] H.T. El-Dessouky, H.M. Ettouney, F. Al-Juwayhel, Multiple effect evaporation—vapour compression desalination processes, Chem. Eng. Res. Des. 78 (4) (2000) 662–676.
[32] H. Kohli, et al., Hybrid desalting technology maximizes recovery, Desalination 56 (1985) 61–68.
[33] D. Han, Study on zero-emission desalination system based on mechanical vapor recompression technology, Energy Procedia 75 (2015) 1436–1444.
[34] V.C. Onishi, et al., Shale gas flowback water desalination: single vs multiple-effect evaporation with vapor recompression cycle and thermal integration, Desalination 404 (2017) 230–248.
[35] T.D. Hayes, et al., Mechanical Vapor Recompression for the Treatment of Shale-Gas Flowback Water, (2014).
[36] P. Horner, B. Halldorson, J.A. Slutz, Shale gas water treatment value Chain – a review of technologies, including case studies, SPE Annual Technical Conference and Exhibition, Society of Petroleum Engineers: Denver, Colorado, USA, 2011.
[37] D. Pierce, K. Bertrand, C. CretiuVasiliu, Water recycling helps with sustainability, SPE Asia Pacific Oil and Gas Conference and Exhibition, Society of Petroleum Engineers: Brisbane, Queensland, Australia, 2010.
[38] V. Fedotov, et al., Water management approach for shale operations in North America, SPE Unconventional Resources Conference and Exhibition-Asia Pacific, Society of Petroleum Engineers: Brisbane, Australia, 2013.
[39] W.F. Heins, R. McNeill, S. Albion, World's first SAGD facility using evaporators, drum boilers, and zero discharge crystallizers to treat produced water, J. Can. Pet. Technol. 45 (5) (2006) 7.
[40] X. Gao, et al., Application of mechanical vapor recompression heat pump to double-effect distillation for separating N,N-dimethylacetamide/water mixture, Ind. Eng. Chem. Res. 54 (12) (2015) 3200–3204.
[41] X. Gao, et al., Application of three-vapor recompression heat-pump concepts to a dimethylformamide–water distillation column for energy savings, Energy Technol. 2 (2014) 250–256.
[42] L. Cao Nhien, et al., Application of mechanical vapor recompression to acetone – methanol separation, Int. J. Chem. Eng. Appl. 5 (2014) 215–218.
[43] A. Karameldin, A. Lotfy, S. Mekhemar, The Red Sea area wind-driven mechanical vapor compression desalination system, Desalination 153 (1) (2003) 47–53.
[44] A.M. Helal, S.A. Al-Malek, Design of a solar-assisted mechanical vapor compression (MVC) desalination unit for remote areas in the UAE, Desalination 197 (1) (2006) 273–300.
[45] L. Liang, D. Han, Energy-saving study of a system for ammonium sulfate recovery from wastewater with mechanical vapor compression (MVC), Res. J. Appl. Sci., Eng. Technol. 3 (11) (2011) 1227–1232.
[46] W.F. Heins, R. McNeill, S. Albion, World's first SAGD facility using evaporators, drum boilers, and zero discharge crystallizers to treat produced water, J. Can. Pet. Technol. 45 (5) (2006) 30–36.
[47] Aspen plus, User guide, Version 10.2, Aspen Tech. Inc., Cambridge, MA, 2000.
[48] Y. Zhou, C. Shi, G. Dong, Analysis of a mechanical vapor recompression wastewater distillation system, Desalination 353 (2014) 91–97.